

# Practical training of stellar interferometry by measuring spectral fringes visibilities

Barata J.<sup>a</sup>, Illarramendi M.A.<sup>a</sup>, Ayesta I.<sup>b</sup>, Grandes J.<sup>a</sup>, Arrospide E.<sup>b</sup>, and Zubia J.<sup>c</sup>

<sup>a</sup>Applied Physics Department

<sup>b</sup>Applied Mathematics Department

<sup>c</sup>Communications Engineering Department

Faculty of Engineering in Bilbao. University of the Basque Country UPV/EHU. Plaza Ingeniero Torres Quevedo 1 48013 Bilbao (Spain)

## ABSTRACT

In this work, we show an experiment in which the analysis of the fringe visibilities at different wavelengths provides information on the spectral morphology of stellar sources. For our purposes, we have inserted a filter wheel between a camera and a telescope obscured by a double-aperture lid for it to operate as a Michelson Stellar interferometer. The wheel allows the use of up to nine astronomical filters. The spectral emission of stellar sources, either single or binary stars, has been simulated by using the light emitted from the output surfaces of two-meter-long polymer optical fibers illuminated by a broadband light-emitting diode. By analyzing the variation of the fringe visibility with the wavelength, we are able to determine the angular size and separation of our light sources, as well as to find the spectral characteristics of the emission of the stars.

**Keywords:** Stellar interferometry, interferometer, spatial coherence, temporal coherence, polymer optical fiber, visibility

## 1. INTRODUCTION

Since Michelson and Pease (1921) managed to measure the diameter of the star Betelgeuse,<sup>1</sup> interferometry-based techniques have been extensively used in optical astronomy. The main advantage of interferometry, where several separate telescopes work together, is that it achieves greater spatial resolution than direct imaging employing a single telescope limited by diffraction effects at the telescope aperture. The range of applications of stellar interferometry is huge: from the measurement of star sizes and the detection of exoplanets/protoplanets to the characterization of multiple stellar systems characterization.<sup>2</sup> Stellar interferometry is of undoubted importance, but teaching this subject constitutes a challenge. The understanding of the operation of optical stellar interferometry requires a solid background on optics and astronomy, besides a certain amount of technical and optical expertise. Therefore, it is not an easy task to teach stellar interferometry to undergraduate and graduate students, especially if one wants to perform experimental activities related to this topic. Only a few experiments have been developed with the purpose of teaching the basic concepts of stellar interferometry: a Michelson-type radio interferometer,<sup>3</sup> interference methods,<sup>4</sup> and optical telescopes covered by a double-aperture lid that employ polymer optical fibers (POFs) illuminated by laser sources simulating stars.<sup>5,6</sup> These activities utilizing POFs were created for our students of the Master of Space Science and Technology of the University of the Basque Country.<sup>7</sup> Their aim is to provide students with the hands-on experience needed to understand the basic concepts of stellar interferometry using a telescope, a digital camera and image-processing tools. In this work, we take a step forward to gain insight into the effect of the light wavelength and its spectral bandwidth

---

Further author information: (Send correspondence to I.M.A.)

B.J.: E-mail: jagoba.barata@ehu.eus

I.M.A.: E-mail: ma.illarramendi@ehu.eus

A.I.: E-mail: igor.ayesta@ehu.eus

G.J.: E-mail: jon.grandes@ehu.eus

A.E.: E-mail: eneko.arrospide@ehu.eus

Z.J.: E-mail: joseba.zubia@ehu.eus

on the interference patterns. Specifically, we have extended the experimental set-up to measure the dependence of fringe visibility on wavelength. The experiment allows one to measure sizes and separations between different extended sources and it can provide information on the spectral morphology of stellar sources. In advanced optical interferometers, such as the Very Large Telescope Interferometer (VLTI), the analyses of visibility as a function of wavelength are performed to obtain more information about complicated stellar systems, such as circumstellar disks.<sup>8</sup>

The contribution starts by summarizing the theory of spatial and temporal light coherence focusing on stellar interferometry. Afterwards, the experimental set-up and the obtained results are described.

## 2. BASIC PRINCIPLES

An optical stellar interferometer is a device that superimposes light beams from a remote source that are gathered by two or more telescopes. A simplified operation of this interferometer can be conducted by covering a single telescope with a lid having two circular pinholes separated by a variable distance called baseline ( $B$ ). The optical principles of this interferometer are based on those of Young's double-slit experiment, in which coherent light coming from each slit is superimposed producing interference patterns (see Fig. 1). The quality of the observed fringe patterns is characterized by the fringe visibility or contrast  $V$ . It is given by:

$$V = \frac{I_{\text{Max}} - I_{\text{Min}}}{I_{\text{Max}} + I_{\text{Min}}} \quad 0 < V < 1, \quad (1)$$

where  $I_{\text{Max}}$  and  $I_{\text{Min}}$  are the maximum and minimum irradiances of the fringe, respectively.<sup>9</sup> A visibility of 1 in an interference fringe implies that the light waves from the two pinholes are perfectly coherent, whereas  $V = 0$  means that the light waves are completely incoherent. For visibility values ranging between 0 and 1, the light waves coming from the pinholes are partially coherent. The visibility values and their variations with the baseline and with the wavelength are strongly dependent on the type of light source.

For an extended source emitting a nearly monochromatic light, the van Cittert-Zernike theorem describes the relationship between the irradiance distribution of the source and the corresponding fringe visibility.<sup>10</sup> In this case, the visibility is inversely proportional to the source size and it depends on its geometry, but not on the observation position. The behavior of the visibility as a function of the source size is a result of the *spatial coherence* of the light across the double-aperture lid. The interference pattern is limited by the diffraction of the light at the circular pinholes and it can be expressed at the plane of observation as follows:<sup>2,10</sup>

$$I(\alpha) = I_0 \left( \frac{J_1(\pi D \alpha / \lambda)}{\pi D \alpha / \lambda} \right)^2 (1 + V_s \cos(2\pi B \alpha / \lambda)), \quad (2)$$

where  $J_1$  is the first-order Bessel function of the first kind,  $D$  is the pinhole diameter and  $\alpha$  is the observation angle. The product  $\alpha B$  is the optical-path difference for small values of  $\alpha$ , and  $I_0$  is a constant.  $V_s$  is the spatial visibility and it can be calculated by applying the van Cittert-Zernike theorem. For instance, if the light source is described as a circular and uniform disk of angular size  $\theta'$ , which is the simplest model to describe the emission of a star, the fringe visibility is given by the following expression:<sup>11</sup>

$$V_s = 2 \left| \frac{J_1(\pi B \theta' / \lambda)}{(\pi B \theta' / \lambda)} \right|. \quad (3)$$

The steady decrease of this function allows the determination of the source size if  $V_s$  is measured as a function of the baseline  $B$ . The easiest procedure for estimating the source diameter is to calculate the lowest value of  $B = 1.22\lambda/\theta'$  for which the interference fringes disappear. In the particular case of a light source consisting of two circular and uniform disks with the same linear size and brightness, e.g. a binary star, the corresponding fringe visibility can be expressed as follows:<sup>5</sup>

$$V_s = \frac{2}{\sqrt{2}} \left| \frac{J_1(\pi B \theta' / \lambda)}{(\pi B \theta' / \lambda)} \right| \left( 1 + \cos(2\pi B \theta'_s / \lambda) \right)^{1/2}, \quad (4)$$

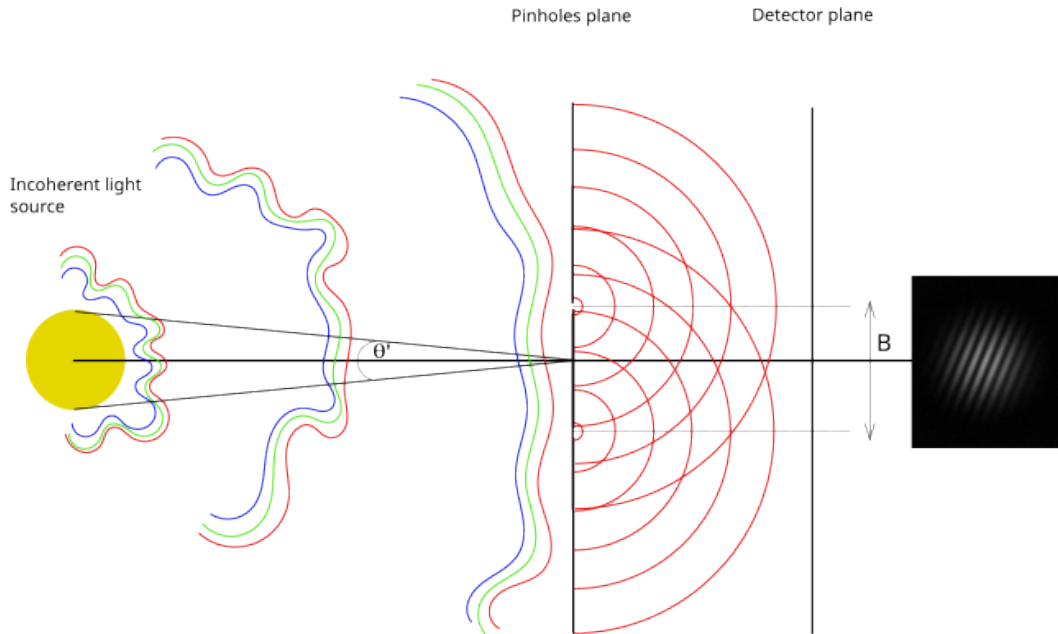


Figure 1. Scheme of a double pinhole stellar interferometer. The two pinholes of diameter  $D$  are separated by a distance  $B$ , and are placed far away from the source.

where  $\theta'_s$  is the angular distance between the components of the binary star, which are placed parallel to the line that joins the two pinholes. This equation expresses that the visibility produced by two identical disks appears as a modulation of the visibility of a single disk shaped by a cosine function. We can easily calculate the angular separation  $\theta'_s$  by measuring the lowest value of  $B$  at which the interference fringes disappear, in which case  $B = \lambda/2\theta'_s$ . It should be noticed that  $V_s$  in Eqs. (3) and (4) does not depend on the observation angle.

For a polychromatic point-light source, it is the Wiener-Khinchin theorem that describes the relationship between the spectral distribution of the source and the fringe visibility.<sup>10</sup> In this case, the visibility depends on the light spectral distribution and on the observation position. The dependence of the fringe visibility on the wavelength distribution is the result of the *temporal coherence* of the light. If we consider that the light spectral distribution is centered at  $\lambda$  with a finite spectral bandwidth  $\Delta\lambda$ , an approximate diffraction-limited fringe pattern could be written as:<sup>2,12</sup>

$$I(\alpha) = I_0 \left( \frac{J_1(\pi D \alpha / \lambda)}{\pi D \alpha / \lambda} \right)^2 (1 + V_t \cos(2\pi B \alpha / \lambda)) \quad \text{with} \quad V_t = 1 - \alpha B \frac{\Delta\lambda}{\lambda^2}. \quad (5)$$

One of the consequences of observing a source with a significant bandwidth is the reduction of visibility as the observation angle  $\alpha$  is increased or, equivalently, as the time delay or the optical path between two beams becomes larger. The time delay for the interference fringes to vanish is called the coherence time, which is defined as the inverse of the frequency bandwidth of the light. In particular, the value of  $V_t$  decreases down to 0 as  $\alpha$  increases up to  $\alpha_c = \lambda^2/B\Delta\lambda$  or as the interference order becomes  $m = \lambda/\Delta\lambda$ . In the event that the values of  $B$  and  $\Delta\lambda$  used in the measurements gave rise to very high values of  $\alpha_c$ , the value of  $V_t$  calculated close to the optic axis on the detector plane would be nearly 1.

The complete description of the interference pattern resulting from an extended multiple-wavelength incoherent source would be obtained by convolving the response of a point source emitting a finite spectral bandwidth

$\Delta\lambda$  with the appropriate spatial source distribution. In summary, the quality of the interference pattern is a combination of the behaviors mentioned in the two previous cases. A rough approximation for the total visibility could be  $V = V_s V_t$ . Hence, the intensity distribution could be expressed as:<sup>2</sup>

$$I(\alpha) = I_0 \left( \frac{J_1(\pi D\alpha/\lambda)}{\pi D\alpha/\lambda} \right)^2 (1 + V_s V_t \cos(2\pi B\alpha/\lambda)), \quad (6)$$

### 3. EXPERIMENTAL SET-UP AND PROCEDURE

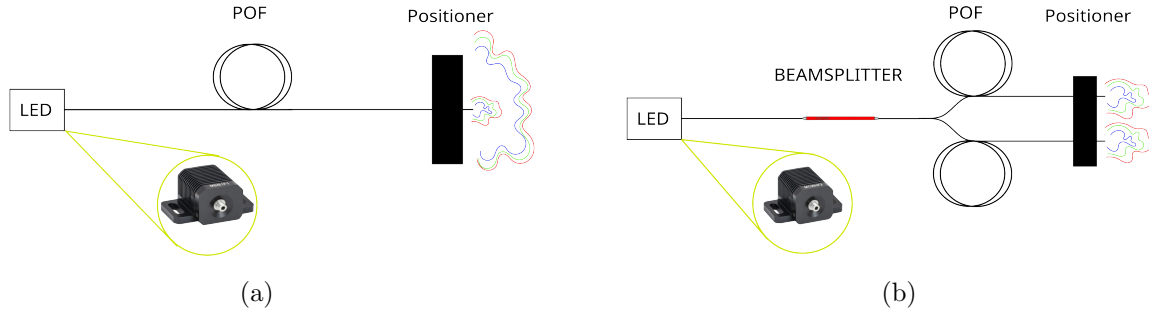


Figure 2. The experimental set-ups that simulate different light sources: (a) Single star with Thorlabs’s MBB1F1 LED ; (b) binary star with Thorlabs’s MCWHF2 LED and Thorlabs’s TM105R5S1A 50:50 beamsplitter.

Fig. 2 shows the schemes of the optical systems designed for the simulation of the spectral emission of stellar sources. To simulate a single star, the light coming from a broadband light-emitting diode (LED) is coupled into a multimode POF. To simulate a binary star, the light of the broadband LED is firstly split into two beams by means of a beam splitter and then the beams are coupled into two POFs through SMA connectors. In both cases, the output fiber ends are inserted into one or two holes located in an L-shape element, named positioner. Multimode POFs have a large core diameter ( $\sim 1$  mm) and a high numerical aperture ( $\sim 0.5$ ). The length of our fibers is 2 m, which is enough for the spatial coherence of the light to be lost,<sup>13,14</sup> so the output fiber ends can be considered as stars, that is, as uniform and spatially and temporally incoherent circular light sources.

The experiments were carried out indoor in low-light conditions. The distance between the interferometer and the light source was  $L = 53 \pm 1$  m. The interferometer used was a Celestron Astromaster 114 EQ Newtonian telescope, with an aperture of 114 mm and a focal length of 1000 mm, covered by a lid with two-pinholes of 2 mm. A filter wheel (1.25” Omegon) was inserted at the optical exit of the telescope, thus allowing us to use up to 9 different filters. Spectral information of the employed optical filters is shown in Tab. 1. The detection of the interference images was carried out by a DMK41AU02 8-bit-dynamic-range camera whose pixel size was  $4.65 \mu\text{m}$ . The experimental setup of the interferometer can be seen in Fig. 3.

The images were processed utilizing the software ImageJ. For each image, a photometric cut perpendicular to the interference pattern was made (see Fig. 4 (a)). The visibility values used to analyze the spectral dependence were calculated using Eq. (1) with  $I_{\text{Max}}$  and  $I_{\text{Min}}$  calculated at observation positions close to the optic axis, as is shown in Fig. 4 (b), where  $I_{\text{Min}}$  is the mean value between the first two interference minima. In that way, we minimize the effects of both the light diffraction and the fringe blurring produced by a finite spectral bandwidth. The final visibility value is calculated as the mean of 5 measurements, and the error of each visibility measurement is the standard deviation.

Table 1. Mean wavelength and spectral width of the optical filters employed in our experiments. The values have been obtained by taking into account the spectral emission of the light source and the spectral responsivity of the camera. The filter shown at the bottom of the table was only used to compare theoretical and experimental photometric cuts. The absolute errors in all cases are  $\pm 1$  nm. The integer  $m$  is the interference order corresponding to the disappearance of the fringes due to the loss of temporal coherence.

Optical filters	MBB1F1		MCWHF2		$m$
	$\lambda$ (nm)	$\Delta\lambda$ (nm)	$\lambda$ (nm)	$\Delta\lambda$ (nm)	
BAADER H- $\beta$ 8.5 nm	489	8	489	8	61
BAADER O-III	501	14	501	14	36
MEADE-Green	540	66	540	67	8
THORLABS FB60010	600	9	600	9	67
619BP5	620	5	620	5	124
635BP5	635	5	636	5	127
BAADER H- $\alpha$ 7 nm	657	7	656	6	94/109
BAADER S-II	673	6	673	6	112
750BP5	749	7	752	7	107
BAADER H- $\alpha$ 35 nm	645	37	642	34	17/19



Figure 3. Experimental set-up of the interferometer.

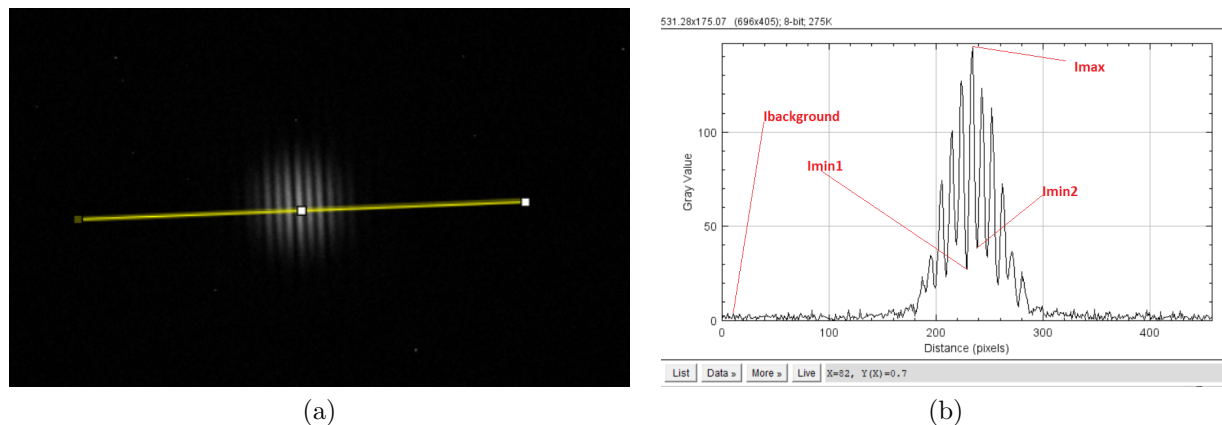


Figure 4. (a) Photometric cut made using the software ImageJ ; (b) Intensity distribution as a function of the distance in pixels.  $I_{\text{Background}}$  is subtracted from  $I_{\text{Max}}$  and  $I_{\text{Min}}$  to calculate visibilities.

#### 4. RESULTS

Fig. 5 shows the effect of the light spectral width  $\Delta\lambda$  on four interference images obtained with three different optical filters (MEADE-Green, BAADER H- $\alpha$  35 nm and BAADER H- $\alpha$  7nm) and also in the absence of a filter. In all cases, the light source is a single star of 1mm and the baseline at the telescope aperture is  $B = 14$  mm. The experimental images and their photometric cuts are displayed in the first and second columns of Fig. 5, respectively. The third column corresponds to the theoretical predictions calculated from Eq. (6).

As can be seen in, the experimental and theoretical photometric curves are in good agreement regarding the number of visible fringes and the values of fringe visibilities, even though the rough approximation  $V = V_s V_t$  has been used for the theoretical predictions. Taking the diffraction effect into account, the number of interference patterns that can be observed can be easily obtained from the angular fringe spacing ( $\lambda/B$ ) and the angular radius of the Airy disk ( $1.22\lambda/D$ ). If the fringes in Fig. 5 were only diffraction limited, the order of the fringes that would not be visible should be 9 in all cases. This effect occurs in the case of the two BAADER filters, it almost occurs with the MEADE-Green filter and it does not happen without filter. In the latter case, with a  $\Delta\lambda$  value close to 200 nm, the fringes are strongly affected by the loss of temporal coherence, resulting in the disappearance of the fringes at the interference order of 4 (Fig. 5(d)). From these results, it can be observed that, for values of  $B$  of 14 mm or smaller,  $V_t$  at observation positions close to the optic axis can be assumed to be 1 when the measurements are performed with the filters of Tab. 1. In other words, the fringe visibility calculated from the central patterns is not affected by the spectral widths of the filters. Therefore, we can use the expressions for the spatial visibility to analyze the spectral dependence of the experimental visibility values calculated at the central fringe.

Fig. 6 shows the evolution of the experimental visibilities with the light wavelength, calculated with a baseline of 14 mm. In (a), the results correspond to a single star of 1 mm, yielding an angular size of 3.9 arcsec. In (b), the data have been obtained with a symmetric binary star in which each component is of 1 mm and the separation is 3 mm, yielding an angular separation of 11.7 arcsec. It must be noticed that the spectral dependence of the visibility with a constant baseline  $B$  changes strongly with the spatial geometry of the light source. The spectral dependence of the visibility for a single circular star shows a slight increase, whereas an abrupt change of slope around a minimum at 525 nm is observed in the case of a binary star. A fit of Eq. (3) to the values displayed in Fig. 6 (a), with  $B = 14$  mm, leads to  $\theta' = 4.1 \pm 0.2$  arcsec, which differs by 5% from its nominal value. When Eq. (4) is fitted to visibility experimental values of the binary star, the results obtained are:  $\theta' = 4.9 \pm 0.4$  arcsec and  $\theta'_s = 11.5 \pm 0.3$  arcsec, which differ by 26% and 2% from nominal values, respectively. The agreement between the nominal data and the experimental results, indicates the validity of the analysis of the fringe visibility as a function of wavelength.

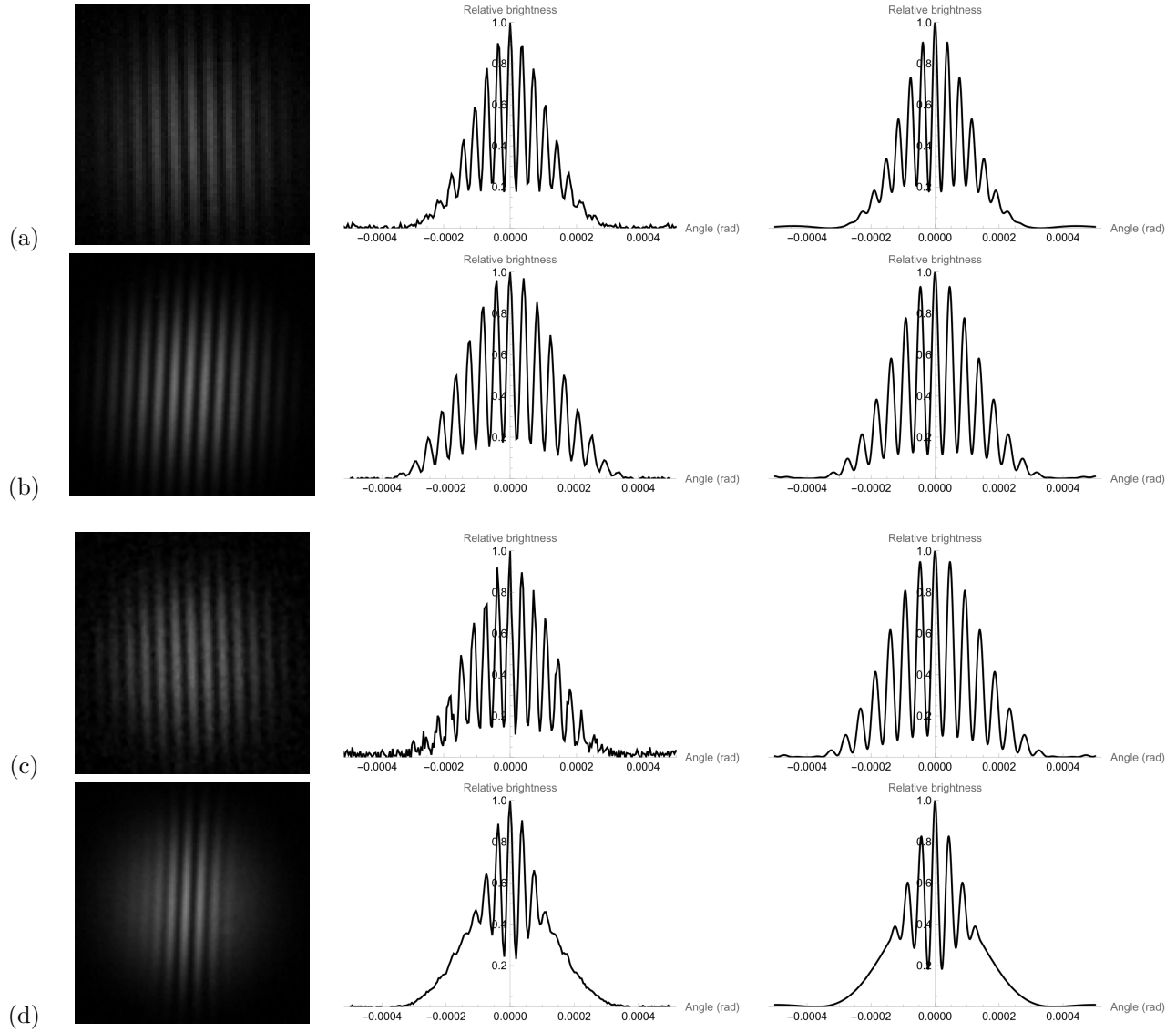


Figure 5. Interference patterns produced in the case of a single star with  $B = 14$  mm. The first and second columns are the experimental images and the photometric cuts, respectively. The third column is the theoretical intensity distribution obtained from Eq. (6). (a) MEADE-Green optical filter ; (b) BAADER H- $\alpha$  35 nm optical filter ; (c) BAADER H- $\alpha$  7 nm ; (d) without optical filter (  $\lambda = 611$  nm and  $\Delta\lambda = 185$  nm).

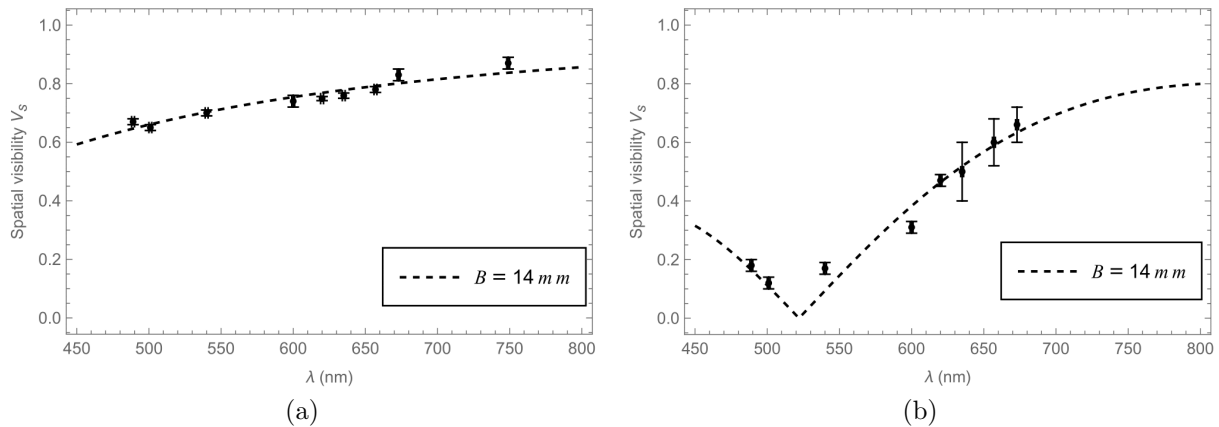


Figure 6. Visibility as a function of wavelength using 14 mm of baseline. Dots are experimental values, whereas the dashed lines are the fittings: (a) single star ; (b) binary star.

## 5. SUMMARY

An experimental set-up that recreates the spectral operation of stellar interferometry has been developed, in which students measure the fringe visibilities as functions of wavelength. The spectral emission of single and binary stars have been simulated using two-meter-long polymer optical fibers illuminated by broadband LEDs, which emit like uniform circular sources of spatially and temporally incoherent light. Light wavelength can be changed by inserting an optical filter wheel at the optical exit of a telescope, which is obscured by a double-aperture lid to operate as a Michelson stellar interferometer. We have shown that the fringe patterns obtained with several optical filters and with no filter are well described by diffraction-limited interference patterns with a fringe visibility related to the loss of the spatial and temporal light coherence. The loss of spatial light coherence is due to the size of the light source, whereas the lack of temporal one arises from the light spectral width. The effect of temporal coherence can be neglected, except when no filter is used, since it has been demonstrated that the fringe visibility calculated close to the optic axis is not affected by the spectral widths of the filters. By analyzing the variation of the spatial fringe visibility with wavelength, we have determined the angular size and the separation of the light sources, with relative errors as smaller as 2%. This type of experiment can be suitable for students and/or teachers in high schools and universities. The didactic nature of the experiment allows underlining important concepts related to stellar interferometry, such as spatial and temporal light coherence, as well as training with the use of telescopes, digital cameras, several astronomical band-pass filters and image processing tools.

## ACKNOWLEDGMENTS

This work has been supported by the following institutions: Spanish “Ministerio de Ciencia e Innovación” under project PID2021-122505OBC31 and Gobierno Vasco/Eusko Jaurlaritza under project IT1452-22.

## REFERENCES

- [1] Michelson, A. A. and Pease, F. G., “Measurement of the diameter of alpha-orionis by the interferometer,” *Proceedings of the National Academy of Sciences* **7**(5), 143–146 (1921).
- [2] Glindemann, A., [*Principles of stellar interferometry*], Springer Science & Business Media (2011).
- [3] Koda, J., Barrett, J., Shafto, G., Slechta, J., Hasegawa, T., Hayashi, M., and Metchev, S., “A michelson-type radio interferometer for university education,” *American Journal of Physics* **84**(4), 249–256 (2016).
- [4] Carbonel, C., Grasset, S., and Maysonnave, J., “Accessing high spatial resolution in astronomy using interference methods,” *The Physics Teacher* **56**(4), 232–234 (2018).
- [5] Arregui, L., Illarramendi, M., Zubia, J., Hueso, R., and Sanchez-Lavega, A., “Interferometry of binary stars using polymer optical fibres,” *European Journal of Physics* **38**(4), 045704 (2017).

- [6] Illarramendi, M., Hueso, R., Zubia, J., Aldabaldetrekue, G., Durana, G., and Sánchez-Lavega, A., “A daylight experiment for teaching stellar interferometry,” *American Journal of Physics* **82**(7), 649–653 (2014).
- [7] Sánchez-Lavega, A., Pérez-Hoyos, S., Hueso, R., del Río-Gaztelurrutia, T., and Oleaga, A., “The aula espacio gela and the master of space science and technology in the universidad del país vasco (university of the basque country),” *European Journal of Engineering Education* **39**(5), 518–526 (2014).
- [8] “ESO - the European Southern Observatory.” <https://www.eso.org/public/chile/?lang>.
- [9] Hecht, E., [*Optics*], Pearson (2012).
- [10] Born, M. and Wolf, E., [*Principles of optics: electromagnetic theory of propagation, interference and diffraction of light*], Elsevier (2013).
- [11] Berger, J. P. and Segransan, D., “An introduction to visibility modeling,” *New Astronomy Reviews* **51**(8-9), 576–582 (2007).
- [12] Pedrotti, F. L., Pedrotti, L. M., and Pedrotti, L. S., [*Introduction to optics*], Cambridge University Press (2017).
- [13] Yoshimura, H., Asakura, T., and Takai, N., “Spatial coherence properties of light from optical fibres,” *Optical and Quantum Electronics* **24**, 631–646 (June 1992).
- [14] Imai, M. and Ohtsuka, Y., “Spatial coherence of laser light propagating in an optical fibre,” *Optical and quantum electronics* **14**(6), 515–523 (1982).